Freeman, H., Scott, A. J., Brydson, R. M. D. (2017): Thermal annealing of nuclear graphite during in-situ electron irradiation. - *Carbon, 115*, pp. 659—664.

DOI: http://doi.org/10.1016/j.carbon.2017.01.057

Thermal annealing of nuclear graphite during in-situ electron irradiation

H. M. Freeman[1,2*], A.J. Scott[1], R.M.D. Brydson[1,3]

1 Institute for Materials Research, School of Chemical and Process Engineering, Univ. Leeds, Leeds LS2 9JT, UK
2 GeoForschungsZentrum, Helmholtz Research Centre Telegrafenberg, 14473 Potsdam, Germany
3 SuperSTEM Laboratory, SciTech Daresbury Laboratories, Daresbury, WA4 4AD, UK

We have investigated the in-situ electron irradiation of nuclear graphite within a 200 kV transmission electron microscope at temperatures between 83 K and 473 K. For each temperature, nuclear grade Pile Grade A graphite specimens were subject to a fluence of ca. 10^{22} electrons cm^{-2}, and transmission electron micrographs and selected area diffraction patterns were collected during electron beam exposure. By considering a critical fluence, at which the graphite (002) *d*-spacing increased by 10%, a temperature threshold for damage has been determined. Below ca. 420 K, electron irradiation caused significant net structural damage: fragmenting basal planes and producing a tortuous nanotexture. Above this temperature the effects of thermal annealing became more prevalent, maintaining the structure even at much higher fluences. We have derived activation energies for the annealing processes operative in these two temperature regimes and, via a comparison with theoretical predictions have, for the first time, associated these with specific recovery processes.

1. Introduction

The majority of the UK's nuclear reactors are graphite-moderated Advanced Gas-Cooled Reactors (AGRs) which operate at temperatures around 625 K in order to reduce the degree of net irradiation damage through continuous thermal annealing. In addition to moderating the energy of fast neutrons so as to control the fission reaction, the graphite provides structural support to the reactor core and allows for coolant flow through a series of channels. Understanding the damage processes occurring in nuclear graphite (NG) during neutron irradiation is essential for the prediction of the lifetime of the material, which in turn influences the overall lifetime of the reactor [1]. A number of studies have been carried out using electron irradiation within a transmission electron microscope (TEM), where electrons are used as a surrogate for neutrons [2–7]. However, many of these studies have been conducted at ambient temperatures. In order to understand the mobility of the atomic structure under irradiation, it is beneficial to perform such in-situ experiments over a range of temperatures.

When investigating new defect structures in graphite, it is common to calculate defect formation energies, defect migration energies, and activation energies for self-diffusion via

* Corresponding author. E-mail: freeman@gfz-potsdam.de. Tel: +49 331 288-1475 (Helen Freeman)

vacancies/interstitials using accurate modelling techniques such as density functional theory [8–12]. The rate of annealing of defects is dependent on activation energy and temperature through the Arrhenius formula (equation 1),

$$\upsilon(T) = A(T)\exp\left({}^{-E_a}/_{(k_B T)}\right) \quad (1)$$

where $\upsilon(T)$ is the migration frequency, $A(T)$ is the vibrational frequency of the defect, and the exponential function describes the defect annealing rate (dependent on the activation energy, E_a, temperature, T, and Boltzmann's constant, k_B). If the activation energy and vibrational frequency of a defect is known, Equation 1 can be used to determine the temperature at which the defect becomes mobile (i.e., when the migration frequency > 0).

Muto & Tanabe investigated the effects of electron irradiation on cleaved graphite thin foils and highly graphitized carbon fibres at both 293 K and also 673 K using TEM, selected area electron diffraction (SAED), and electron energy loss spectroscopy (EELS) [7]. After 1 hour of 200 kV electron beam exposure at the two differing temperatures, SAED patterns (along [001]) showed significant differences: irradiation at 293 K resulted in diffuse rings whereas irradiation at 673 K gave sharp polycrystalline Debye-Scherrer rings. TEM images and SAED patterns (along [100]) also provided evidence for temperature-dependent structural changes. Bending and/or breaking of lattice fringes were observed following electron beam exposure at 673 K, however the (002) basal plane spacing derived from TEM images and diffraction patterns showed no change. EEL C K-edge spectral series during electron irradiation at 673 K showed little change, indicating that the hexagonal structure within basal planes was maintained. In contrast, the C K-edge spectra from 293 K electron irradiation exhibited significant changes in the π^* and σ^* peaks which was identified with the formation of non-hexagonal (e.g. 5 or 7 membered) atomic rings. They proposed that the damage process above 673 K involved recrystallisation of the structure.

Burden & Hutchison exposed specimens of "KS10" grade graphite particles (highly graphitized carbon with a particle size of 10 μm) to a 400 kV electron beam (10^{19} electrons $cm^{-2}s^{-1}$) at 293 K and 773 K [6]. At 293 K crystalline particles deteriorated to amorphous spheres of up to 50 nm in diameter. However at 773 K the structural stability was significantly improved so that the specimen could be exposed for much longer (1200 s) without the formation of disordered carbonaceous spheres. It was suggested this was due to thermal energy providing the ability to resist and simultaneously repair damage.

Nakai *et al.* investigated the effect of electron irradiation (at energies between 0.1 and1.0 MeV) on HOPG over a range of temperatures, from 113 K to 473 K [5]. TEM images, SAED patterns (along [001]), and EEL spectra were all collected. The fluence threshold for so called "amorphization" was measured for each temperature, where amorphization was recognised as the formation of diffuse rings in a [001] SAED pattern. For fluxes of ca. 10^{19} electrons $cm^{-2}s^{-1}$ the fluence threshold gradually increased for increasing temperature, and increased significantly above 420 K.

To further explore the temperature threshold for net damage and also the activation energies of defects, in situ electron irradiation of nuclear graphite over a variety of temperatures has been undertaken. Collecting lattice images and their fast Fourier transform (FFT) patterns during 200 kV beam exposure has provided evidence for a temperature threshold for damage which is in broad agreement with previous studies.

Small interstitial loops (radius < 100 Å) have been observed to form during neutron irradiation at temperatures below 923 K and these are expected to migrate and potentially coalesce at temperatures above 1273 K [13,14]. It was therefore expected that thermal annealing would reduce the overall damage rate, and that a temperature threshold for damage could be deduced [5,15]. To decide on a suitable temperature range over which electron irradiation studies should be performed, the migration energies of single interstitials and vacancies were considered. The migration energy of a single interstitial has been theoretically calculated to be ca. 1.5 eV [9], but experimental results show a much smaller value of < 0.4 eV [16]. Converting these energies to a temperature via the Arrhenius formula (equation 1) gives a large temperature range of between 143 K and 546 K (assuming $\upsilon(T)$ = 1 migration per second and $A(T) = 10^{14}$ Hz [9,13]). The single vacancy has been calculated to have a migration energy of 1.1 eV, corresponding to a temperature of 400 K [8,10,12,17]. The migration energy of a single interstitial depends on its configuration (e.g. grafted, dumbbell or spiro) and varies between 0.1 eV and 2.2 eV [10,16,18–21]. Experiments were therefore conducted at 83 K, 293 K, 373 K, 423 K and 473 K.

2. Experimental

In situ heating experiments were performed using a DENS Solutions in-situ TEM holder in an FEI Tecnai TEM at an operating voltage of 200 kV providing an electron flux of approximately 10^{19} electrons $cm^{-2}s^{-1}$ [22]. Pile Grade A (PGA) graphite was ground and dispersed in acetone and drop cast directly onto the DENS chip which was then placed in the holder and inserted into the microscope. The chips are ca. 1 cm in length with a spiralled micro-hotplate (300 μm ×300 μm) at the centre using four-point resistive temperature feedback. This makes for accurate temperature

readings at the centre of the chip (< ± 5%), high temperature stability, and offers a ramp rate capability of 200 K per millisecond. Furthermore, the combination of the high thermal conductivity of graphite and the holder's four-point resistive feedback to measure temperature means the temperature reading reflects the temperature of the specimen. In situ heating experiments were performed at 373 K, 423 K and 473 K. The imaging conditions were exceptionally stable and drift was minimal, allowing the same area to be studied both before and during heat treatment. The high thermal conductivity of graphite means that the localised heating effects from the electron beam were considered to be negligible [23].

In-situ cooling experiments (83 K) were performed using a Gatan 636 double tilt cooling holder, whereas a conventional Gatan TEM holder was used for room temperature studies. All sample and microscope operating conditions were the same as for the heating experiments.

To measure the change in (002) *d*-spacing following electron beam exposure, lattice images and their corresponding FFTs were collected; measurements were calibrated against SAED patterns. To quantify the degree of structural change observed in TEM lattice images following electron radiation, 2D image analysis software provided by the PyroMaN research group at the University of Bordeaux was employed [24]. A discussion of the capabilities of this software and its application to room temperature electron irradiation of PGA graphite is given in reference [3]. Based on an analysis of (002) lattice fringes, the software provides information on fringe length, and tortuosity using Fourier transform filtering and a level curve tracking algorithm [25]. Although the algorithm detects fringes even if they exceed the image boundaries, these longer fringes cannot be included in the measurements since the true length and tortuosity cannot be determined; therefore micrographs exhibiting little structural change could not be quantified via this method.

3. Results

Graphite (002) lattice images were collected at regular intervals during electron irradiation providing a large set of images as a function of total fluence. Specifically, in Figure 1, we show for comparison the set of HRTEM images of NG samples both before and after an electron fluence of between 10^{21} - 10^{23} electrons cm^{-2} for the range of different temperatures studied. Before electron beam exposure, basal planes exhibited long range order. Low temperature electron irradiation induced fragmentation of the basal planes and produced a tortuous nanotexture. At higher temperatures (> 420 K) the effects of thermal annealing became more prevalent, demonstrated through the preservation of a layered structure even for much higher fluences.

In Figure 2 the change in (002) *d*-spacing (as measured from image FFTs) as a function of electron fluence is shown for the range of temperatures studied. After initial exposure to the electron beam at 83 K and also 293 K, the *d*-spacing increases rapidly, particularly for the lower temperature. Linear fits have been added to all data sets; at both 373 K and 423 K the *d*-spacing initially stays constant up until a threshold fluence where it begins to increase at a rate of ca. 0.03 nm per 10^{22} electrons cm^{-2}, in these cases, the linear fit was applied to the data after the threshold fluence. At 473 K the *d*-spacing does not significantly change with electron fluence. The R^2 values for each linear fit have been determined; for 83 K, 293 K and 423 K the R^2 values are >0.92 showing a good linear fit of data points. For the 373 K data the R^2 value of the linear fit is 0.78 due to higher variability in the measured *d*-spacing; in 3 instances, data points and their error bars lie outside the linear fit. Furthermore, this data set deviates from a linear trend which could be fitted by a polynomial (to the power of 2) however such changes to the fit do not significantly change the critical fluence (i.e. the point at which the line of best fit crosses the line showing a 10% increase in *d*-spacing). Due to the shallow gradient of the 473 K data set the R^2 is very low, however the linear fit crosses all data points' error bars. The delayed structural change observed in midrange temperatures is in agreement with the findings of Kelly *et al.* [26] who exposed pyrolytic graphite to neutron irradiation at different temperatures. It is thought that this delay period reflects a balance in the damage and annealing processes; at a certain point the effects of irradiation damage begin to outweigh the effects of thermal annealing which is reflected through an increase in *d*-spacing.

The PyroMaN analysis technique used to quantify changes in (002) fringe length and tortuosity can only be applied to the micrographs collected at 83 K, 293 K, 373 K and 423 K. At 473 K and above, the basal planes largely extend beyond the image boundaries limiting the accuracy of the extractable data from the PyroMaN software. For all analysed data sets, the lengths of fringes decreased by ca. 60% and the levels of tortuosity increased to >1.14 after a fluence of 4×10^{22} electrons cm^{-2}. This provides evidence that at temperatures ≤ 423 K, electron irradiation-induced net structural damage occurs.

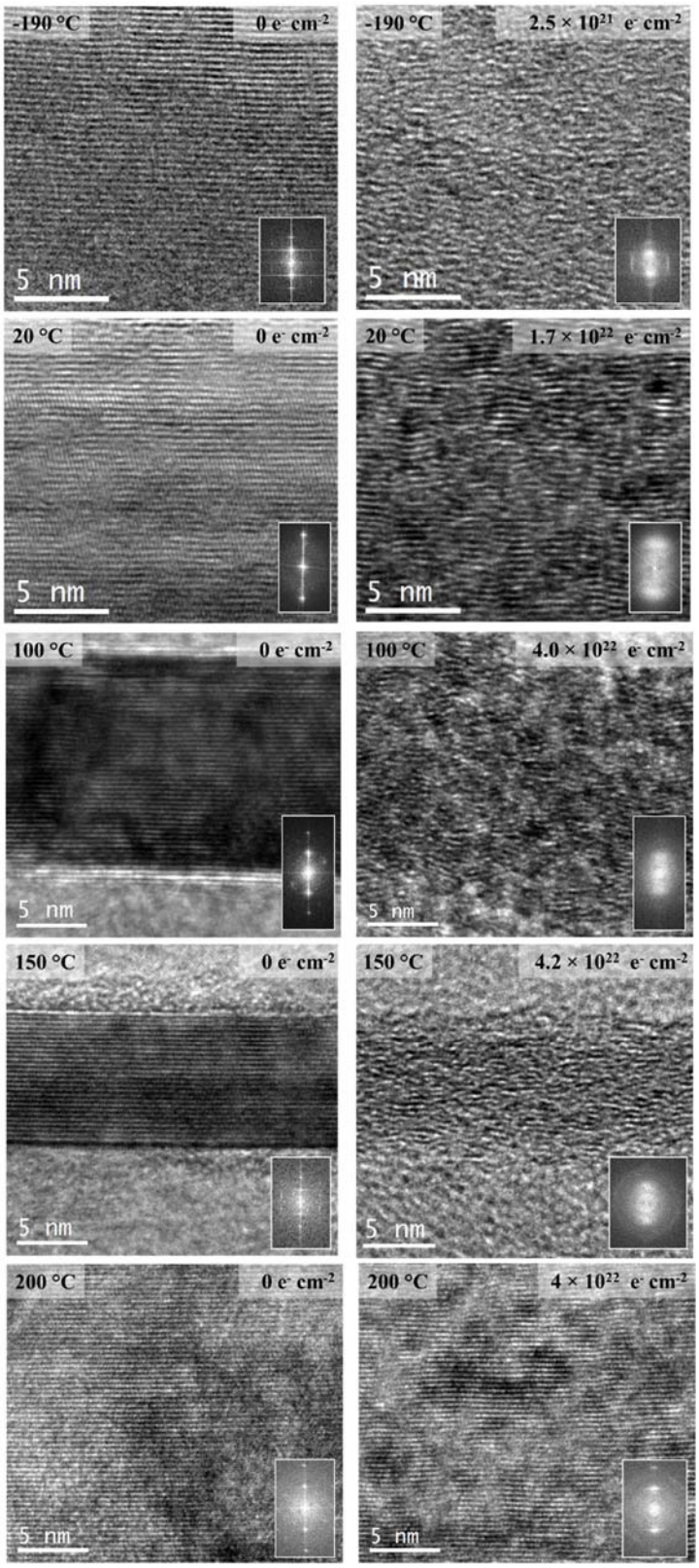

Figure 1 TEM micrographs and their corresponding FFT patterns before and after 200 kV electron beam exposure at 83 K, 293 K, 373 K, 423 K and 473 K.

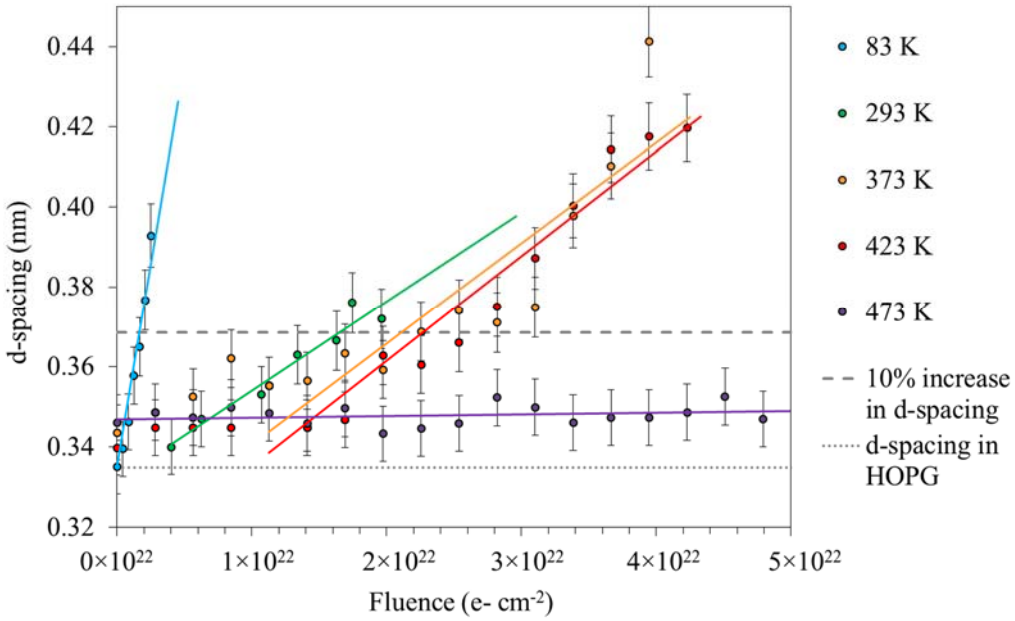

Figure 2 Change in (002) *d*-spacing with electron fluence at 200 kV electron beam exposure at 83 K, 293 K, 373 K, 423 K and 473 K. The two horizontal lines indicate the (002) *d*-spacing in HOPG and a 10% increase in *d*-spacing which are used as reference points. Error bars reflect standard experimental error of measuring *d*-spacing from FFTs [3].

4. Discussion

To interpret a temperature threshold for net (electron) irradiation damage from these results, a critical fluence at each temperature was determined. The critical fluence was arbitrarily defined as the fluence at which the (002) *d*-spacing increased by 10%. Due to the low net damage rates at 200°C, this data set was extrapolated (from Figure 2) to predict the fluence at which a 10% change in *d*-spacing would have occurred. Muto & Tanabe performed a similar analysis based on [001] SAED patterns collected for different temperature in situ electron irradiation experiments [7]. In their study, the fluence was measured in terms of 'displacements per atom' (dpa) and was referred to as a dose. The method of conversion from e^- cm^{-2} to dpa was not disclosed in the report. However, previous studies by the same authors [27] used a conversion factor of 10^{-23} cm^2, or 10 barns, which according to the McKinley-Feshbach formula and Figure 18 in [28], corresponds to a displacement threshold energy of 25 eV. Muto & Tanabe defined the critical fluence as the fluence at which the [001] diffraction pattern transformed into (polycrystalline) Debye-Scherrer rings. To compare the two sets of data, the fluence thresholds determined in this study were converted to dpa units. For consistency, we used the same displacement threshold energy and corresponding cross section as Muto & Tanabe (25 eV and 10 barns respectively). Multiplying the fluence in e^- cm^{-2} by the displacement cross section gives a value for the fluence in dpa.

Figure 3 presents the data of Muto & Tanabe as well as our current data, measured at 83 K, 373 K, 423 K and 473 K plus data at room temperature from a previous publication by the authors [3,7]. This is displayed as an Arrhenius-type plot and in both data sets there is a clear point at which the gradient changes. This discontinuity indicates there is a change in the annealing/radiation damage process at a certain temperature. For the data in this study and that from the work of Muto & Tanabe, this change occurs at ca. 420 K and ca. 400 K respectively. The difference in these values may be a result of different critical fluence definitions, different specimens, and/or the slightly different electron fluxes used. Both data sets have been extrapolated to predict the critical fluence at 623 K (1.6×10^{-3} K^{-1}) in order to reflect the environment of a nuclear reactor (ca. 625 K). However, since the temperature threshold is associated with the gradient change, the different critical fluence definitions are not expected to be a significant contributor to the discrepancy between the two data sets as this will only alter the position of the graph on the ordinate. Other methods which could be employed to calculate a critical fluence include the possibility of monitoring changes in the relative proportion of planar sp^2 bonded carbon atoms using core loss EELS (e.g. when the carbon sp^2 content drops to 80%) or by measuring changes in (002) fringe length and orientation [3,24].

The temperature threshold of ca. 420 K determined from Figure 3 is within the accuracy of density functional theory calculations of Latham *et al.* who estimated that the temperature threshold for a vacancy migration to occur at a rate of 1 s^{-1} was 396-411 K (E_a = 1.1 eV) [12]. The recombination of Frenkel pairs, as a result of vacancy mobility suggests that above ca. 420 K the hexagonal structure within basal planes would be maintained and is largely unchanged by radiation [20] in agreement with our present observations. The observation of the fragmentation and curvature of basal planes in TEM micrographs collected during electron irradiation below ca. 420 K, along with an increase in *d*-spacing, provides evidence that any annealing effects are outweighed by radiation damage at these lower temperatures.

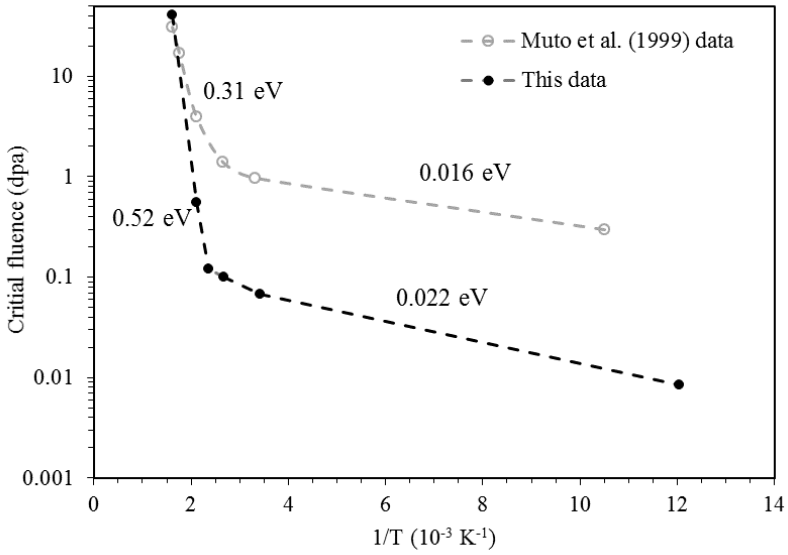

Figure 3 Arrhenius plot of the critical fluence for different temperatures, with corresponding activation energies labelled. Data is plotted from this study and from that presented by Muto & Tanabe [7]. Data sets have been extrapolated to show the critical fluence at 623 K (1.6×10^{-3} K^{-1}).

To better understand the thresholds derived from Figure 3 and those discussed in the literature, the migration energies of various defect configurations should be considered. Experiments measuring the electrical resistance and lattice parameters of a variety of low temperature, radiation exposed graphite grades have resulted in a range of values for the single interstitial migration energy (0.04 - 0.4 eV) [16]. However, theoretical calculations for such energies are consistently higher (1.2 - 2 eV) [9,17,29]. It has been proposed that these discrepancies are due to a simplified interpretation of the indirect experimental results, in particular the effect of shear on the derived migration energies not being accounted for [9,17,30].

Assuming the data in Figure 3 indeed follows the Arrhenius law (equation 1), the gradient from each of the two distinct sections of the graph can be used to derive E_a for the thermally assisted recovery process that is operative in each temperature range. This is because the ordinate is the critical fluence required to promote damage, which is a measure of the resistance to electron beam induced damage. The activation energies above and below the threshold temperature for the data in this study were calculated to be 0.022 eV and between 0.53 - 1.03 eV respectively. The latter data range reflects the values derived from different extrapolations of the T = 473 K data in Figure 2; one with a constrained y-axis intercept of 0.335nm, the value for virgin graphite (0.53 eV), and one for a trend line with no fixed intercept (1.03 eV). For the data extracted from Muto & Tanabe these values are 0.016 eV and 0.31 eV, however they drew no specific conclusions about the significance of their

results. Due to a lack of data points, the errors on these calculations are quite high; nevertheless, the values from both data sets are of a similar magnitude.

As discussed, it is expected that at temperatures below the ca. 420 K threshold, the effects of radiation damage dominate so that the net effect is relatively fast structural damage. The calculated low activation energy for thermal annealing (0.016 - 0.022 eV) reflects an easy, yet relatively ineffectual damage recovery process. The derived activation energies allow us to determine which defect structures are mobile and therefore aid the recovery of radiation damage in each temperature range. The annealing of structural changes induced by low temperature irradiation $\leq$ 420 K may be a result of surface or interfacial atomic diffusion at crystallite boundaries where the diffusion coefficients would be expected to be at least an order of magnitude above bulk volume diffusion. It is widely accepted that radiation exposure can result in the diffusion of surface atoms even if energies below the displacement threshold are transferred [31]. The reported radiation-induced fragmentation of crystallites (and consequent formation of grain boundaries) [7,27,32] would increase the internal surface area therefore increasing the possibility of atomic mobility through diffusion. Such surface atoms would be able to fill vacant sites on surfaces, but not those in between planes (which would require higher energies). However, despite these recovery processes, the effects of radiation damage are dominant resulting in a net structural damage. Above 420 K, the effects of thermal annealing become more prevalent which is reflected through an increased thermal annealing activation energy (0.31 - 0.53 eV) that indicates that another mechanism is coming into play. The mobility of defects in this temperature range would allow the structure to recover within the bulk crystallites; in addition to surface migration, the mobility of both single interstitials and vacancies through the lattice could lead to Frenkel pair recombination.

The high operating temperatures of AGRs (ca. 625 K) therefore reduces overall damage rates, however the long duration of radiation exposure means that structural damage would still be expected to occur. Extrapolation of data in Figure 3 gives a critical fluence at 623 K (1.6×10^{-3} K^{-1}) of 25 - 30 dpa. A speculative calculation, assuming the flux in a graphite moderated nuclear reactor is 10^{-7} dpa s^{-1} [4], would infer such a fluence would occur after ca. 1 year (although this value is highly dependent on the value used for displacement energy threshold in calculating the fluence in dpa). Similarly, a graphite moderated reactor operating temperature of 723 K would increase this speculative critical fluence limit to 3 years. However, it must be noted that typical graphite moderated nuclear reactors are operated at full power for up to 3 years then undergo a 2-3 month maintenance down time period before resuming the cycle. The lifetime usually quoted for reactors does not usually take this into account, meaning the full power lifetime is smaller. Furthermore, the

c-axis expansion is expected to plateau and not increase indefinitely [26]. Therefore it is likely that effects of the critical fluence (i.e. a 10% increase in *d*-spacing) will be experienced beyond the times quoted. It would also be interesting to see if a third phase of behaviour is experienced for higher temperatures; new designs for the graphite moderated reactors employ temperatures of around 1173 K where different temperature/radiation induced property changes would be expected to occur.

5. Conclusion

Electron irradiation of PGA graphite within a transmission electron microscope has been investigated for five temperatures: 83 K, 293 K, 373 K, 423 K and 473 K. Analysis of TEM lattice images and FFT patterns showed that temperature strongly affected the structural degradation during electron exposure and a temperature threshold was determined by considering the variation of the critical fluence for damage, as defined by a certain set of criteria. Below ca. 420 K, electron irradiation significantly damaged the atomic structure and was accompanied by fragmented basal planes, a tortuous nanotexture, and a >10% increase in *d*-spacing. Above ca. 420 K the effects of thermal annealing became more prevalent preserving the structure to much higher fluences. The activation energies above and below this temperature threshold were calculated to be 0.022 eV and 0.53 eV respectively and are thought to reflect two different mechanisms for thermal annealing one involving surface diffusion which is relatively ineffectual and a second involving migration of Frenkel pairs leading to significant structural recovery.

Acknowledgements

Funding was provided by the National Nuclear Laboratory and EPSRC (grants EP/J502042/1). H.M. Freeman would like to acknowledge the Helmholtz Recruiting Initiation funding for Liane G. Benning. Jean-Pierre Da Costa and the late Patrick Weisbecker provided us access to the PyroMaN image analysis software and acknowledge support from the ANR agency through a grant to the program ‘‘PyroMaN’’ (ANR-BLAN-2010-0929).

References

[1] R.E. Nightingale, Nuclear Graphite, Academic Press, 1962.

[2] S. Muto, S. Horiuchi, T. Tanabe, Local structural order in electron-irradiated graphite studied by high-resolution high-voltage electron microscopy, J. Electron Microsc. (Tokyo). 48 (1999) 767–776. doi:10.1093/oxfordjournals.jmicro.a023747.

[3] B.E. Mironov, H.M. Freeman, A.P. Brown, F.S. Hage, A.J. Scott, A.V.K. Westwood, J.-P. Da Costa, P. Weisbecker, R.M.D. Brydson, Electron irradiation of nuclear graphite studied by transmission electron microscopy and electron energy loss spectroscopy, Carbon N. Y. 83 (2015) 106–117. doi:10.1016/j.carbon.2014.11.019.

[4] C. Karthik, J. Kane, D.P. Butt, W.E. Windes, R. Ubic, In situ transmission electron

microscopy of electron-beam induced damage process in nuclear grade graphite, J. Nucl. Mater. 412 (2011) 321–326. doi:10.1016/j.jnucmat.2011.03.024.

[5] K. Nakai, C. Kinoshita, A. Matsunaga, A study of amorphization and microstructural evolution of graphite under electron or ion irradiation, Ultramicroscopy. 39 (1991) 361–368. doi:10.1016/0304-3991(91)90216-S.

[6] A.P. Burden, J.L. Hutchison, Real-time observation of fullerene generation in a modified electron microscope, J. Cryst. Growth. 158 (1996) 185–188. doi:10.1016/0022-0248(95)00547-1.

[7] S. Muto, T. Tanabe, Fragmentation of graphite crystals by electron irradiation at elevated temperatures, J. Electron Microsc. (Tokyo). 48 (1999) 519–523.

[8] T. Trevethan, P. Dyulgerova, C.D. Latham, M.I. Heggie, C.R. Seabourne, A.J. Scott, P.R. Briddon, M.J. Rayson, Extended interplanar linking in graphite formed from vacancy aggregates, Phys. Rev. Lett. 111 (2013) 95501. doi:10.1103/PhysRevLett.111.095501.

[9] L. Li, S. Reich, J. Robertson, Defect energies of graphite: Density-functional calculations, Phys. Rev. B. 72 (2005) 1–10. doi:10.1103/PhysRevB.72.184109.

[10] H. Zhang, M. Zhao, X. Yang, H. Xia, X. Liu, Y. Xia, Diffusion and coalescence of vacancies and interstitials in graphite: A first-principles study, Diam. Relat. Mater. 19 (2010) 1240–1244. doi:10.1016/j.diamond.2010.06.010.

[11] C.D. Latham, M.I. Heggie, J. a Gámez, I. Suárez-Martínez, C.P. Ewels, P.R. Briddon, The di-interstitial in graphite, J. Phys. Condens. Matter. 20 (2008) 395220. doi:10.1088/0953-8984/20/39/395220.

[12] C.D. Latham, M.I. Heggie, M. Alatalo, S. Oberg, P.R. Briddon, The contribution made by lattice vacancies to the Wigner effect in radiation-damaged graphite., J. Phys. Condens. Matter. 25 (2013) 135403. doi:10.1088/0953-8984/25/13/135403.

[13] R.H. Telling, M.I. Heggie, Radiation defects in graphite, Philos. Mag. 87 (2007) 4797–4846. doi:10.1080/14786430701210023.

[14] P.A. Thrower, Interstitial loops in graphite, their motion and their effect on elastic modulus, Philos. Mag. 16 (1967) 189–209. doi:10.1080/14786436708229268.

[15] W.N. Reynolds, Physical properties of graphite, Elsevier Publishing Co. LTD, 1968.

[16] P.A. Thrower, R.M. Mayer, Point defects and self-diffusion in graphite, Phys. Status Solidi. 47 (1978) 11–37. doi:10.1002/pssa.2210470102.

[17] A. El-Barbary, R. Telling, C. Ewels, M. Heggie, P. Briddon, Structure and energetics of the vacancy in graphite, Phys. Rev. B. 68 (2003) 1–7. doi:10.1103/PhysRevB.68.144107.

[18] A. Gulans, A. Krasheninnikov, M. Puska, R. Nieminen, Bound and free self-interstitial defects in graphite and bilayer graphene: A computational study, Phys. Rev. B. 84 (2011) 1–6. doi:10.1103/PhysRevB.84.024114.

[19] Y. Ma, Simulation of interstitial diffusion in graphite, Phys. Rev. B. 76 (2007) 75419. doi:10.1103/PhysRevB.76.075419.

[20] E.W.J. Mitchell, M.R. Taylor, Mechanism of stored-energy release at 200° C in electron-irradiated graphite, Nature. 208 (1965) 638–641. doi:10.1038/208638a0.

[21] R.H. Telling, C.P. Ewels, A.A. El-Barbary, M.I. Heggie, Wigner defects bridge the graphite gap., Nat. Mater. 2 (2003) 333–7. doi:10.1038/nmat876.

[22] DENS Solutions, Nano-Chip Technology, (2015). www.denssolutions.com/products/nano-chip/ (accessed May 6, 2015).

[23] D.B. Williams, C.B. Carter, Transmission electron microscopy: A textbook for materials science, 2nd ed., Springer, 2009.

[24] J.P. DaCosta, P. Weisbecker, B. Farbos, J.-M. Leyssale, G.L. Vignoles, C. Germain, Investigating carbon materials nanostructure using image orientation statistics, Carbon N. Y. 84 (2015) 160–173. doi:10.1016/j.carbon.2014.11.048.

[25] J.-P. DaCosta, C. Germain, P. Baylou, Level curve tracking algorithm for textural feature extraction, in: S.Y. Sanfeliu A, Villanueva JJ, Vanrell M, Alquzar R, Crowley J (Ed.), 15th Intl. Conf. Pattern Recognit., Los Alamitos, CA: IEEE, Barcelona, 2000: pp. 909–912. doi:0-7695-0750-6/00.

[26] B.T. Kelly, W.H. Martin, P.T. Nettley, Dimensional changes in pyrolytic graphite under fast-neutron irradiation, Philos. Trans. R. Soc. London A. 260 (1966) 37. doi:10.1098/rsta.1966.0028.

[27] M. Takeuchi, S. Muto, T. Tanabe, S. Arai, T. Kuroyanagi, Damage process in electron-irradiated graphite studied by transmission electron microscopy. II. Analysis of extended energy-loss fine structure of highly oriented pyrolytic graphite, Philos. Mag. A. 76 (1997) 691–700. doi:10.1080/01418619708214030.

[28] O. Oen, Cross sections for atomic displacements in solids by fast electrons, Oak Ridge National Laboratory ORNL-3815, 1965.

[29] M.I. Heggie, I. Suarez-martinez, C. Davidson, G. Haffenden, Buckle , ruck and tuck : A proposed new model for the response of graphite to neutron irradiation, J. Nucl. Mater. 413 (2011) 150–155. doi:10.1016/j.jnucmat.2011.04.015.

[30] K. Niwase, Irradiation-induced amorphization of graphite: A dislocation accumulation model, Philos. Mag. Lett. 82 (2002) 401–408. doi:10.1080/09500830210137416.

[31] F. Banhart, Irradiation effects in carbon nanostructures, Reports Prog. Phys. 62 (1999) 1181–1221. doi:S0034-4885(99)97991-5.

[32] N.C. Gallego, R.A. Meisner, T.D. Burchell, Annealing studies of irradiated HOPG using X-ray measurements, in: Int. Nucl. Graph. Spec. Meet., IAEA Knowledge Base on Nuclear Graphite, Seattle, 2013. web.ornl.gov/sci/physical_sciences_directorate/mst/.../pdf/paper36_Gallego.pptx.